

Real-time spectroscopic ellipsometry as a characterization tool for oxide molecular beam epitaxy

B. J. Gibbons, M. E. Hawley, S. Trolier-McKinstry, and D. G. Schlom

Citation: *Journal of Vacuum Science & Technology A* **19**, 584 (2001); doi: 10.1116/1.1351054

View online: <http://dx.doi.org/10.1116/1.1351054>

View Table of Contents: <http://scitation.aip.org/content/avs/journal/jvsta/19/2?ver=pdfcov>

Published by the AVS: Science & Technology of Materials, Interfaces, and Processing

Articles you may be interested in

[In situ spectroscopic ellipsometry in plasma-assisted molecular beam epitaxy of InN under different surface stoichiometries](#)

J. Appl. Phys. **99**, 044913 (2006); 10.1063/1.2172703

[Real-time composition control of InAlAs grown on InP using spectroscopic ellipsometry](#)

J. Vac. Sci. Technol. B **18**, 1435 (2000); 10.1116/1.591398

[Real-time composition control using spectral ellipsometry in growth of Hg_{1-x}Cd_xTe by molecular beam epitaxy](#)

J. Vac. Sci. Technol. B **18**, 1381 (2000); 10.1116/1.591389

[Characterization of strained Si/Si_{1-y}C_y structures prepared by molecular beam epitaxy](#)

J. Vac. Sci. Technol. B **16**, 1621 (1998); 10.1116/1.589846

[Real-time diagnostics of II-VI molecular beam epitaxy by spectral ellipsometry](#)

J. Vac. Sci. Technol. A **15**, 216 (1997); 10.1116/1.580515



Advance your technology or engineering career using the **AVS Career Center**, with **hundreds of exciting jobs** listed each month!

<http://careers.avs.org>



Real-time spectroscopic ellipsometry as a characterization tool for oxide molecular beam epitaxy

B. J. Gibbons^{a)}

Superconductivity Technology Center, Los Alamos National Laboratory, Los Alamos, New Mexico 87545

M. E. Hawley

Structure-Property Relations Group, Los Alamos National Laboratory, Los Alamos, New Mexico 87545

S. Trolier-McKinstry and D. G. Schlom

The Pennsylvania State University, University Park, Pennsylvania 16802

(Received 14 January 2000; accepted 8 January 2001)

A real-time spectroscopic ellipsometer (RTSE) was designed and implemented on an oxide molecular beam epitaxy (MBE) system. The RTSE was designed as a complementary tool to the other existing *in situ* deposition monitors on the MBE. To quantify how the RTSE complemented the other tools (as well as to determine its limitations), the RTSE was used to characterize the deposition of (111)-oriented Y_2O_3 on (111) Si and (110)-oriented Y_2O_3 on (100) Si. Results from computer modeling of the RTSE data subsequent to deposition showed excellent agreement with atomic absorption flux measurements, quartz crystal monitor flux measurements, reflection high energy electron diffraction measurements, and Rutherford backscattering spectroscopy. From the RTSE measurements, growth rates and microstructures were determined and verified by *ex situ* techniques. In addition, the sticking coefficient of yttrium to Y_2O_3 was found to be 1.00 ± 0.07 . Also, the temperature dependent optical properties of the Y_2O_3 films were measured at 25 and at 730 °C. Nearly bulk values were found, indicating the high quality films deposited via this method.

© 2001 American Vacuum Society. [DOI: 10.1116/1.1351054]

I. INTRODUCTION

Spectroscopic ellipsometry (SE) is a light reflection technique which is capable of depth profiling samples with a resolution that depends somewhat on the material being studied, but is typically in the angstrom range. SE is nondestructive, noninvasive, and requires no sample preparation. Basically, the measurement involves determining the change in polarization state of a light beam of known wavelength and polarization state upon reflection from the sample surface. This change (represented in the measured ellipsometric parameters, Δ and Ψ) is related to the depth profile of the dielectric function of the sample.¹ Computer modeling can then be utilized to obtain a best-fit description of the sample detailing the optical properties as a function of depth.²⁻⁵ Excellent agreement between SE and other techniques such as cross-sectional transmission electron microscopy (TEM),⁶ atomic force microscopy (AFM),^{7,8} secondary ion mass spectroscopy,⁹ and Rutherford backscattering spectroscopy (RBS)¹⁰ has been demonstrated. Originally, SE was used to study static materials with the goal of characterizing the depth profile and optical properties. With the advent of high-speed computers, and innovations in detector technology and usage, SE has been extended to the study of dynamic processes occurring during thin film deposition.

The technique of real-time spectroscopic ellipsometry (RTSE) using silicon photodiode array detectors has matured significantly since its development over ten years ago.^{8,11} In addition to this type of RTSE, there have been instruments

developed based on other detection and polarization generation methods.^{12,13} Here, we will focus on the silicon photodiode array-based RTSE. The ability to collect full spectroscopic spectra (1.5 to 3.5 eV) with an acquisition time of as little as 16 ms resulted in $<1\text{-\AA}$ -thickness resolution for growth rates up to 60 $\text{\AA}/\text{s}$. With these capabilities, RTSE has been applied to characterization of the nucleation, coalescence, and growth processes of amorphous and crystalline thin films. In addition, the evolution of the optical properties of these materials as a function of thickness at different growth stages has been determined.¹⁴⁻¹⁸

In this work, an RTSE was constructed and adapted for use on an oxide molecular beam epitaxy (MBE) deposition system. The RTSE was designed as a complementary tool to the other existing *in situ* deposition monitors on the MBE, including atomic absorption (AA) flux monitoring, quartz crystal (QCM) flux monitoring, and reflection high energy electron diffraction (RHEED). This was the first time that RTSE has been applied to the deposition of oxide films by MBE, thus here its usefulness, limitations, and how it complements the other *in situ* techniques was examined. These attributes were determined by observing the deposition of epitaxial Y_2O_3 thin films on (100)- and (111)-oriented silicon substrates.

II. EXPERIMENTAL PROCEDURE

A. MBE description

The MBE used for this work is an EPI (Minneapolis, MN) model 930. A diagram of the MBE is given in Fig. 1. There are eight effusion cells available for the deposition of a wide

^{a)}Electronic mail: gibbons@lanl.gov

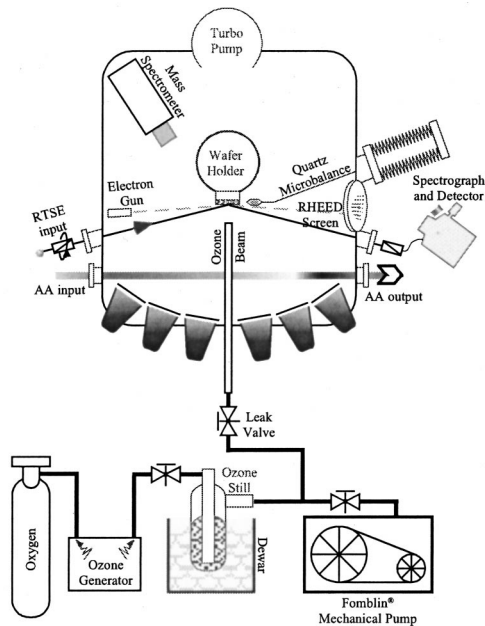


FIG. 1. Schematic of the MBE used in this work.

variety of materials. Here, only the yttrium source was utilized. The yttrium (99.9% pure, Alfa/AESAR) was contained in a tungsten crucible and heated by an EPI “high-temperature” effusion cell capable of source temperatures up to 2000 °C. During film deposition, purified ozone was used as the oxidant. Output from a commercial ozone generator (Model G1-L, PCI Ozone Corp., West Caldwell, NJ) was distilled using a still constructed based on the work of Schlom and Harris.¹⁹ The ozone was leaked into the chamber through a needle valve and released through a nozzle aimed directly at a substrate 8 cm away from the nozzle outlet. The purity of the ozone at the substrate position has been measured and was found to be $\approx 80\%$,²⁰ since a portion of the ozone is broken down to molecular oxygen as it travels from the still to the substrate. In the MBE, the source fluxes were measured using hollow cathode lamp-based atomic absorption spectroscopy (Intelligent Sensor Technologies, Mountain View, CA) during the deposition and quartz crystal microbalance measurements prior and subsequent to deposition. In addition to the *in situ* flux monitoring capability, the MBE also has a RHEED system for structural analysis during deposition (Staib Instrumente, Langenbach, Germany, and *k*-Space, Ann Arbor, MI).

B. RTSE design

The ellipsometer used in this work is a rotating polarizer-sample-fixed analyzer ($P_{\text{rot}}SA$) configuration constructed specifically for this MBE system. A schematic of the RTSE is shown in Fig. 2 (the vacuum chamber is not included for clarity). It is a third generation instrument based on that of Collins.¹¹ White light with a spectral range from the near UV to the near IR is generated by the Xe arc lamp (Hamamatsu Corp., Bridgewater, NJ) and focused onto a 1 mm pinhole. The light is then sent through a UV achromat (Optics for

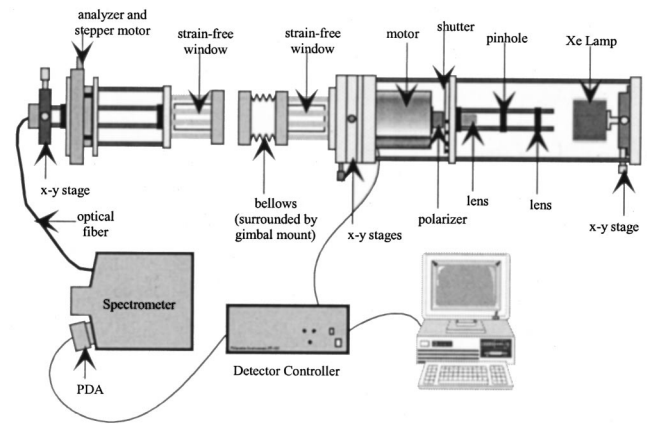


FIG. 2. Schematic of the RTSE used in this work.

Research, Caldwell, NJ) and linearly polarized by the rotating polarizer (motor from Airex Corp., Dover, NH). The polarizer and analyzer in this system are Glan-Taylor prisms (Zeta International Corp., Mt. Prospect, IL). This type of polarizer does not exhibit any optical activity effect, thus no corrections need to be made in the data analysis. The beam enters and exits the vacuum chamber via strain-free windows attached to 2.75 in. ConFlat[®] flanges (Bomco, Inc., Gloucester, MA). After reflection from the sample within the vacuum chamber, the beam passes through the fixed analyzer and is focused onto a 0.6-mm-diam $f/4$ optical fiber (Fiber-guide Industries, Stirling, NJ) which is mated to an $f/4$ spectrograph (SPEX, Edison, NJ). At the spectrograph exit port, a flat focal plane (25 mm wide) is generated where the detector is placed. The detector is a 1024 element photodiode array (PDA) and each element is $25 \mu\text{m} \times 2.5 \text{ mm}$ (Princeton Instruments, Trenton, NJ). It has a saturation count level of 2^{16} and single-pixel and full-array read times of $5 \mu\text{s}$ and 5 ms, respectively.²¹ The diffraction grating used here has 147 grooves/mm and is blazed at 300 nm. This results in a linear dispersion across the PDA of 23.6 nm/mm. Since each pixel is $25 \mu\text{m}$ across, a resolution of 0.59 nm/pixel is obtained. However, the width of the entrance slit of the spectrograph also influences the resolution of the instrument. For a width of 0.15 mm, the resolution is 3.5 nm; for a width of 0.25 mm, the resolution decreases to 5.9 nm, thus in this case the resolution is limited by the slit width. The spectral range for this work is 280–650 nm (1.9–4.4 eV). The RTSE is controlled via software developed by one of the authors²² using Microsoft’s Visual C++ Developer’s Studio[®] and LabWindows/CVI[®] from National Instruments. It is important to note that the performance of the system described here (specifically the detector) shows a significant improvement over the previous two generations of RTSE’s based on this design methodology.^{8,11} Specifically, the image persistence level and the nonlinearity of the detector were dramatically improved with the components used here.

C. Data modeling

For each data set obtained during deposition, 40 optical cycles were averaged and the repetition time of the measure-

ment was 4 s. The ellipsometric data were modeled as a number of discrete layers, each with a specific thickness, density, and wavelength dependent refractive index (the modeling was typically completed after the film deposition). The dispersion behavior $[n(\lambda)]$ was fit to a Sellmeier oscillator function and the goodness of the fit to the measured ellipsometric data (Δ and Ψ) was judged using an unbiased estimator of the error, σ , where

$$\sigma = \frac{1}{N-P-1} \left[\sum_{i=1}^N (\cos \Delta_{\text{exp}}^i - \cos \Delta_{\text{calc}}^i)^2 + (\tan \Psi_{\text{exp}}^i - \tan \Psi_{\text{calc}}^i)^2 \right]^{1/2} \quad (1)$$

Here, N is the number of data points taken (2 for each pixel) and P is the number of unknown variables in the model. The subscripts exp and calc represent the experimental and calculated values of Δ and Ψ , respectively.

Other characterization techniques included atomic force microscopy (AFM), using a Digital Instruments Nanoscope IIIa in tapping mode. For structural analysis, four-circle x-ray diffraction was used. Finally, Rutherford backscattering spectroscopy (RBS) was used for compositional analysis.

D. Substrate preparation and temperature calibration

The silicon substrates were prepared using an RCA clean.²³ The ozone background pressure during the deposition was 1×10^{-6} Torr and the substrate temperature was 720–740 °C. This temperature was determined by SE using the well-defined structures observed in the dielectric spectra of silicon. Specifically, the 3.375 eV feature has been found to decrease linearly (in energy position) with increasing temperature for $80^\circ\text{C} \leq T \leq 550^\circ\text{C}$ according to²⁴

$$E(\text{eV}) = 3.375 - 4.07 \times 10^{-4} [T(^\circ\text{C})]. \quad (2)$$

Here, as in previous work, it is assumed that the linear behavior extends to higher temperatures, as well.^{24,25} An advantage to this method is that the penetration depth of the light in Si at this energy is only 220 Å.²⁵ Therefore, the SE-determined temperature is a true surface temperature.

E. Deposition details

Note that the native oxide on the silicon wafer was *not* completely removed prior to initiating growth. The presence of the amorphous SiO₂ layer is indicated by the absence of an initial RHEED pattern. This layer was also modeled using the RTSE and found to be on the order of 15 Å thick. The yttrium flux was typically set to between $(5 \text{ and } 7) \times 10^{13}$ atoms/cm² s. The method used to deposit Y₂O₃ on silicon is based on the work of Goettler, Maria, and Schlom²⁶ and McKee and Walker.^{27,28} Initially, a dose of 2.0×10^{15} Y atoms/cm², which corresponds to the yttrium content in 3 ML of Y₂O₃, is supplied to the substrate surface in a background pressure of about 1×10^{-8} Torr. Note that this relatively high background pressure for a MBE system is a result of this MBE not being baked as it is dedicated to the growth

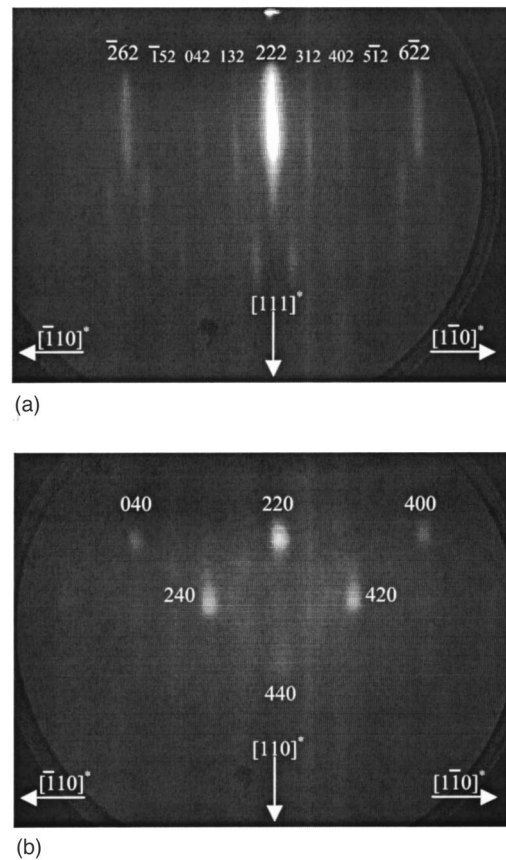


Fig. 3. (a) Final RHEED image of a (111)-oriented Y₂O₃ film grown on (111) Si. The image was taken along the $[11\bar{2}]_{\text{Si}}$ azimuth. (b) Final RHEED image of a (110)-oriented Y₂O₃ film grown on (100) Si. The image was taken along the $[001]_{\text{Si}}$ azimuth. The RHEED peaks are indexed in both images, as are several reciprocal lattice directions of the Y₂O₃ films.

of oxides. Following yttrium exposure, a RHEED pattern indicating the formation of ordered Y₂O₃ at the substrate surface appears. At this point, the main shutter (which blocks the substrate from exposure to all of the sources including the ozone nozzle) is closed and ozone is introduced into the chamber. When the ozone background pressure is stabilized to 1×10^{-6} Torr, the main shutter and the yttrium shutter are opened simultaneously and deposition proceeds until the desired thickness is achieved.

III. RESULTS AND DISCUSSION

Figure 3(a) shows the RHEED pattern at the end of the growth of a 825 Å thick Y₂O₃ film on (111) Si. It indicates that the (111) Y₂O₃ plane is oriented parallel to the (111) plane of the silicon substrate (i.e., (111)-oriented Y₂O₃), and confirms that the growth is epitaxial. Figure 3(b) gives similar data for a 1330 Å thick (110)-oriented epitaxial Y₂O₃ film grown on (100) Si. The spottiness of this RHEED pattern indicates a transmission diffraction pattern through (110)-oriented Y₂O₃, i.e., that the surface of the (110) Y₂O₃ is not smooth on an atomic scale and contains asperities that the electron beam can penetrate through.

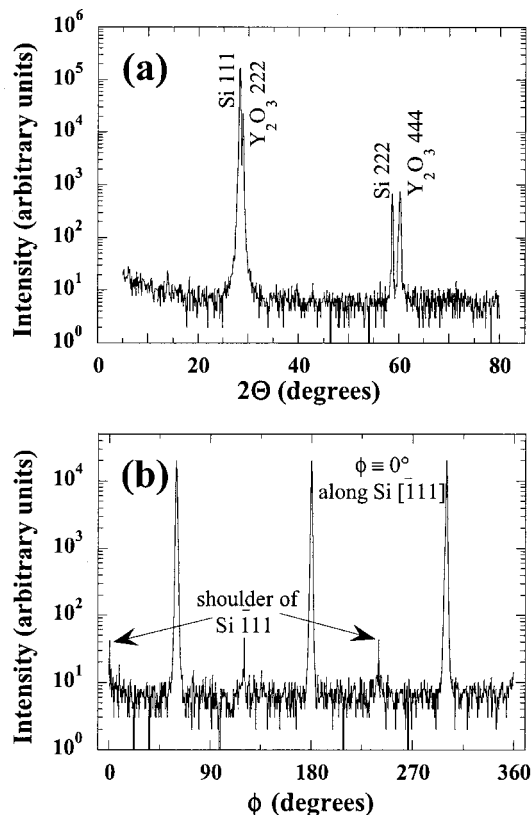


FIG. 4. (a) θ - 2θ x-ray measurements for a (111)-oriented Y_2O_3 film grown on (111) Si. The full width at half maximum of the Y_2O_3 222 peak is 0.31° . (b) A ϕ scan of the Y_2O_3 222 peak.

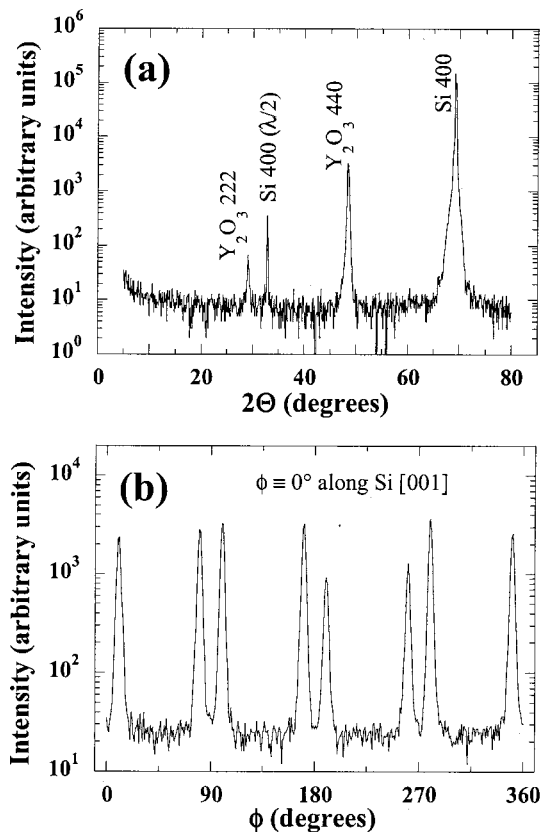


FIG. 5. (a) θ - 2θ x-ray measurements for a (110)-oriented Y_2O_3 film grown on (100) Si. The full width at half maximum of the Y_2O_3 440 peak is 0.49° . (b) A ϕ scan of the Y_2O_3 404 peak.

Figure 4(a) shows the θ - 2θ x-ray measurement of the (111)-oriented film. The presence of sharp peaks in the x-ray pattern in conjunction with the streaks in the RHEED pattern suggest that the film surface is smooth. Figure 4(b) is a ϕ scan of the $\bar{2}22$ Y_2O_3 peak, indicating the film is epitaxial. The smaller peaks in that figure arise from the shoulder of the $\bar{1}11$ peak of the silicon substrate. Figure 5(a) shows x-ray measurements for the film deposited on (100)-oriented silicon. In this case, the film is $>95\%$ (110)-oriented Y_2O_3 , with a small fraction of (111)-oriented Y_2O_3 . Figure 5(b) is a ϕ scan of the 404 Y_2O_3 peak of the (110)-oriented Y_2O_3 , which makes up the majority of the film. This scan indicates that the film has 90° rotation twins. One of the twins has an epitaxial relationship with silicon of $(110)_{\text{Y}_2\text{O}_3} \parallel (100)_{\text{Si}}$ and $[001]_{\text{Y}_2\text{O}_3} \parallel [011]_{\text{Si}}$. The other is $(110)_{\text{Y}_2\text{O}_3} \parallel (100)_{\text{Si}}$ and $[001]_{\text{Y}_2\text{O}_3} \parallel [0\bar{1}1]_{\text{Si}}$.

Two such degenerate epitaxial orientations are expected²⁹ for the growth of a film orientation with twofold symmetry, i.e., (110) Y_2O_3 , on a substrate surface with fourfold symmetry, i.e., (100) Si, and the specific orientation relationships observed are consistent with previous experimental reports.^{30–32}

Real-time SE data for the growth of the film shown in Figs. 3(b) and 5 are given in Fig. 6. Here, the silicon ellipsometric spectra at the growth temperature can be seen prior to initiation of deposition (characterized by the peaks in Δ

between 300 and 400 nm at time=0). At the onset of growth, those peak heights in Δ decrease rapidly. Thus, it is clear that the magnitude of these peaks at a given temperature is very sensitive to the presence of an overlayer. During the deposition, the development of interference fringes can be seen in the data. This is due to the interference between reflections from the surface of the growing Y_2O_3 film and the interface between the Y_2O_3 and silicon.

After deposition, the RTSE data were modeled at various points throughout the deposition sequence. In addition, after removal of the sample from the MBE, *ex situ* ellipsometric data were obtained to confirm the results of the RTSE analysis. The results of the *ex situ* modeling are given in Fig. 7. Several geometries were attempted for the modeling; including those with an SiO_2 layer at the interface, or surface roughness, or a low density layer at the interface. The best-fit geometry for these data did not include any surface roughness or an interfacial layer. This is in contrast to similar work performed by Bardal *et al.*^{33,34} In that work, a ≈ 20 Å thick layer of an undetermined phase was observed by TEM at the interface between (110) Y_2O_3 and (100) Si.

In Fig. 7, the film thickness was determined to be $1330 \text{ \AA} \pm 3 \text{ \AA}$ from modeling the *ex situ* SE spectra. The fits are very good, with a final σ value of 0.048 and very low correlations between variables. Modeling the final RTSE

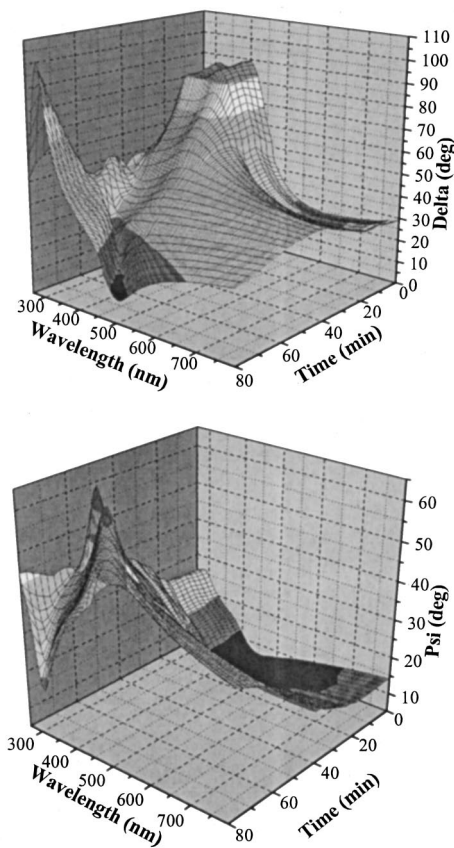


FIG. 6. RTSE data for (110) Y_2O_3 deposition on (100) Si.

spectra at the growth temperature resulted in a film thickness of $1325 \text{ \AA} \pm 11 \text{ \AA}$ ($\sigma=0.062$). The evolution in thickness determined from modeling the RTSE spectra during deposition is given in Fig. 8. Again, the best-fit models did not include any surface roughness. Based on these data, a deposition rate of 11.2 \AA/min was extracted. In addition, the fitted line has an intercept of $\approx 0 \text{ \AA}$, as is expected. Since the repetition time of the measurement was 4 s, this corresponds to a spectrum of data taken every 0.75 \AA .

Similar analysis was performed on the (111)-oriented Y_2O_3 film deposited on (111)-oriented silicon. In this case, a growth rate of 13.7 \AA/min was extracted. The final thickness obtained by SE was $825 \text{ \AA} \pm 11 \text{ \AA}$ ($\sigma=0.066$), and again, surface roughness or an interfacial SiO_2 layer did not improve the fits significantly. A very smooth surface was also implied by the RHEED pattern. In order to corroborate these surface roughness results, AFM measurements were collected on the (111)-oriented film. These results are given in Fig. 9. The rms roughness value was 2.7 \AA , confirming the RHEED and SE results. The inability to detect this very thin layer of roughness in the SE analysis was due to excessive correlation between variables when roughness was introduced into the model. The final thickness obtained by measuring the flux by QCM before and after deposition was $850 \text{ \AA} \pm 40 \text{ \AA}$ (assuming a 5% variability in the flux determined by the QCM³⁵), showing good agreement [similar measurements were collected on the (110)-oriented film and

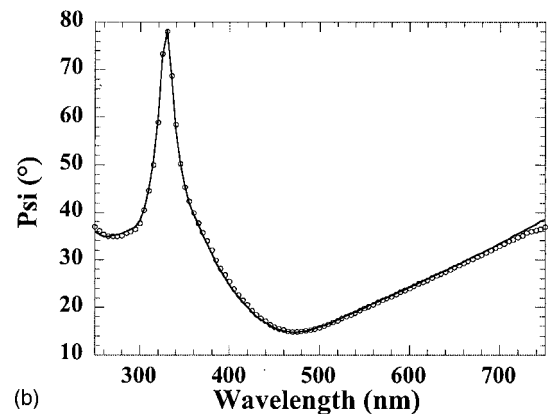
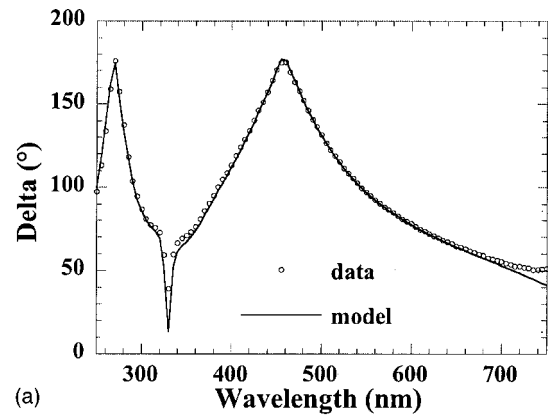


FIG. 7. *Ex situ* ellipsometric data and model for a (110)-oriented Y_2O_3 film grown on (100) Si.

agreement was achieved between the RHEED, AFM, and RTSE results].

One of the key goals of this work was to determine how RTSE could be used to complement the existing *in situ* diagnostic tools. In particular, AA measurements describe the flux which is incident on the substrate, while SE is sensitive to the species which are incorporated into the film. Consequently, comparison of the two numbers enables the sticking coefficient to be calculated. This was done as follows for the (110)-oriented Y_2O_3 film:

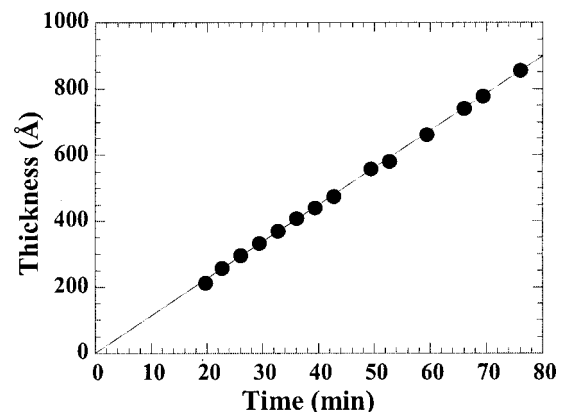


FIG. 8. Best-fit film thicknesses determined from analysis of RTSE data taken during the deposition of (110) Y_2O_3 on (100) Si.

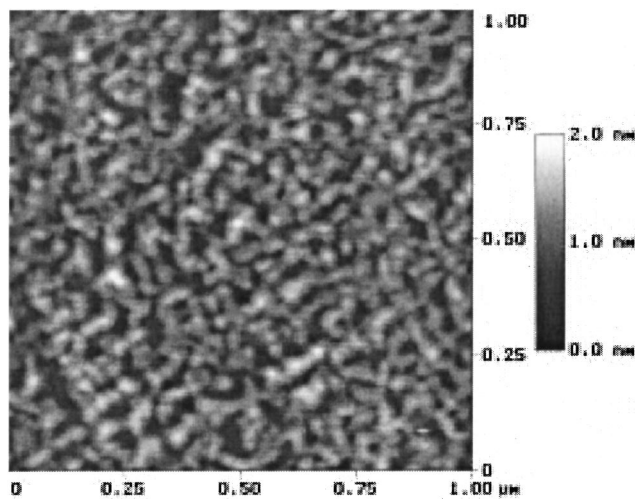


FIG. 9. AFM image of a (111) Y_2O_3 film on (111) Si. The rms roughness value is 2.7 \AA .

- (1) Y flux (measured by AA) = $4.94 \times 10^{13} \text{ atoms/cm}^2 \text{ s}$;
- (2) shutter open = 6952 s;
- (3) total Y dose = $3.4 \times 10^{17} \text{ atoms/cm}^2$ and

$$(4) \text{ thickness by AA} = \frac{3.4 \times 10^{17} \text{ atoms/cm}^2 \left[\frac{10.6 \text{ \AA}}{4 \text{ ML}} \right]}{7.1 \times 10^{14} \text{ atoms/ML}} \\ \approx 1280 \text{ \AA} \pm 30 \text{ \AA}.$$

This is in comparison to the RTSE obtained film thickness of $\approx 1325 \text{ \AA} \pm 11 \text{ \AA}$. Using the RTSE-determined deposition rate, and the time the shutter was open, a final film thickness of 1300 \AA is found. For a direct comparison, the same sample was analyzed using Rutherford backscattering spectroscopy (RBS). Results from these measurements give an absolute quantification of the amount of yttrium and oxygen in the thin film. For this sample, there was found to be $3.34 \pm 0.10 \times 10^{17} \text{ Y atoms/cm}^2$ and $5.00 \pm 0.28 \times 10^{17} \text{ O atoms/cm}^2$. Based on these values, and assuming a bulk density of 5.01 g/cm^3 ,³⁶ a thickness of $1250 \text{ \AA} \pm 30 \text{ \AA}$ is obtained. Thus, the agreement between AA (calibrated with the QCM), RTSE, and RBS is excellent. In addition, the agreement between SE (which is sensitive to the incorporation of flux in the film) and AA (which is a measure of the flux to the film surface) indicates that the sticking coefficient of yttrium in Y_2O_3 is $\approx 1.00 \pm 0.07$.

The ability of RTSE to measure the sticking coefficient holds some advantages over other methods. For instance, when the QCM is used to measure the sticking coefficient, the fact that the QCM is water cooled must be accounted for. For elements with appreciable re-evaporation rates (i.e., lead and bismuth), this is significant. That is, when the same element is deposited on a hot substrate, the sticking coefficient is likely to be less than that measured by the QCM (at a much lower temperature). For this case, RTSE can directly measure the amount of incorporated species on the hot substrate. In addition, in certain cases, there are changes in the deposition rates when two species are deposited together

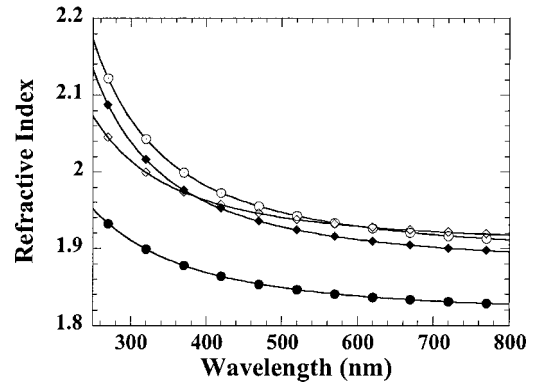


FIG. 10. Comparison of refractive index values for bulk Y_2O_3 (\circ) (see Ref. 37), epitaxial Y_2O_3 grown on (110) Si at its growth temperature of $730 \text{ }^\circ\text{C}$ (\diamond) and after cooling to room temperature (\blacklozenge), and evaporated Y_2O_3 from Feldman and co-workers (\bullet) (see Ref. 38).

with respect to delivering them independently. Since RTSE gives both thickness and optical properties, it should be good for composition determination even in this case. Finally, some elements are not well suited to AA analysis using conventional hollow cathode lamps at low deposition rates typical for MBE (e.g., titanium, lanthanum, and aluminum); the signal to noise ratio of the absorption values is much too low to accurately quantify the flux. In this case, RTSE can be extremely helpful for flux calibration.

From the SE analysis subsequent to deposition, the optical properties of the sample were obtained at the deposition temperature, as well as room temperature. This was done using a Sellmeier oscillator to model the dispersion of the refractive index. In the models, no amount of absorption was detected, indicating the film is well oxidized. The values were compared to bulk values obtained by measurement of the Brewster angle in reflection and by interferometry.³⁷ This comparison is shown in Fig. 10, along with the high temperature data and values from evaporated Y_2O_3 films deposited by Feldman, Ying, and Farabaugh.³⁸ It should be noted that the values of Feldman and co-workers are very similar to other studies on Y_2O_3 thin films.^{39–41} It can be seen that previous results on Y_2O_3 films show very low refractive index values compared to bulk. The authors attributed the lower values to second phase formation, changes in film stoichiometry, stress, and observed extended lattice constants. The films from this work show values much closer to those of the bulk. The data for the MBE-deposited film at its growth temperature of $730 \text{ }^\circ\text{C}$ show a shift in the onset of absorption to lower wavelengths and an increase in the magnitude of the refractive index.

From the x-ray diffraction data presented in Fig. 5, lattice constants of $10.59 \text{ \AA} \pm 0.06 \text{ \AA}$ for the c axis (which lies in the plane of the substrate) and $10.63 \text{ \AA} \pm 0.02 \text{ \AA}$ for the a and b axes were determined, compared to $a = 10.604 \text{ \AA}$ for the bulk (cubic) material.⁴² This corresponds to a density of $4.99 \pm 0.05 \text{ g/cm}^3$ (compared to 5.01 g/cm^3 for the bulk material). From a volume fraction analysis, it can be calculated that $\approx 0.5\%$ air mixed with bulk Y_2O_3 is needed to bring the bulk density down to the value obtained for the film. Using

Bruggeman effective medium averaging to generate refractive index values, it can be shown that mixing 1.5% air with the bulk refractive index curve brings it down to the observed film values. This slightly lower density is believed to be the source of the lower refractive index values observed for the epitaxial Y_2O_3 films grown here compared to bulk Y_2O_3 .

IV. CONCLUSIONS

RTSE has been successfully applied to the deposition of Y_2O_3 by MBE. The RTSE was shown to complement AA, RHEED, and QCM measurements in various ways. In addition, the results of the RTSE analysis were confirmed by RBS experiments on the deposited films. The microstructures and growth rates of the films were determined. In addition, the sticking coefficient of yttrium in Y_2O_3 was determined. Extension of this technique to other oxide materials should prove useful for understanding the growth mechanisms and surface roughness development of these films.

ACKNOWLEDGMENTS

B. J. G. would like to thank Dr. Robert W. Collins for several helpful discussions throughout the progression of this work. Also, the authors gratefully acknowledge Dr. Larry McIntyre of the University of Arizona for the RBS analysis and the financial support of the Office of Naval Research through Grant No. N00014-94-0815.

- ¹R. M. A. Azzam and N. M. Bashara, *Ellipsometry and Polarized Light* (Elsevier, London, 1972).
- ²D. E. Aspnes, in *Optical Properties of Solids, New Developments*, edited by B. O. Seraphin (North-Holland, Amsterdam, 1976), pp. 799–846.
- ³K. Vedam, P. J. McMarr, and J. Narayan, *Appl. Phys. Lett.* **47**, 339 (1985).
- ⁴G. E. Jellison and B. C. Sales, *Appl. Opt.* **30**, 4310 (1991).
- ⁵M. Schubert, B. Rheinländer, J. A. Woolam, B. Johs, and C. M. Herzinger, *J. Opt. Soc. Am.* **13**, 875 (1996).
- ⁶P. J. McMarr, K. Vedam, and J. Narayan, *J. Appl. Phys.* **59**, 694 (1986).
- ⁷G. Zavala, J. H. Fendler, and S. Trolier-McKinstry, in *Ferroelectric Thin Films V*, edited by S. B. Desu, R. Ramesh, B. A. Tuttle, R. E. Jones, and I. K. Yoo, *MRS Symposium Proceedings* (Materials Research Society, Pittsburgh, 1996), Vol. 433, pp. 437–442.
- ⁸R. W. Collins, I. An, H. Fujiwara, J. Lee, Y. Lu, J. Koh, and P. I. Rovira, *Thin Solid Films* **313**, **314**, 18 (1998).
- ⁹S. Trolier-McKinstry and J. Koh, in *Electrically Based Microstructural Characterization*, edited by R. A. Gerhardt, S. R. Taylor, and E. J. Garboczi, *MRS Symposium Proceedings* (Materials Research Society, Pittsburgh, 1995), Vol. 411, pp. 185–190.
- ¹⁰M. Fried, T. Lohner, W. A. M. Aarnink, L. J. Hanekamp, and A. van Silfhout, *J. Appl. Phys.* **71**, 2835 (1992).

- ¹¹R. W. Collins, *Rev. Sci. Instrum.* **61**, 2029 (1990).
- ¹²G. E. Jellison and F. A. Modine, *Appl. Opt.* **29**, 959 (1990).
- ¹³B. Johs, D. Doerr, S. Pittal, and J. A. Woollam, *Surf. Coat. Technol.* **62**, 680 (1993).
- ¹⁴H. V. Nguyen and R. W. Collins, in *Physics of Thin Films*, edited by K. Vedam (Academic, San Diego, 1994), Vol. 19, pp. 127–190.
- ¹⁵R. W. Collins, I. An, H. V. Nguyen, Y. M. Li, and Y. Lu, in Ref. 14, pp. 49–125.
- ¹⁶G. N. Maracas, J. L. Edwards, K. Shiralagi, K. Y. Choi, R. Droopad, B. Johs, and J. A. Woolam, *J. Vac. Sci. Technol. A* **10**, 1832 (1992).
- ¹⁷D. E. Aspnes, *Thin Solid Films* **233**, 1 (1993).
- ¹⁸J. Rivory, S. Fisson, V. Van Nguyen, G. Vuye, Y. Wang, F. Abelés, and K. Yu-Zhang, *Thin Solid Films* **233**, 260 (1993).
- ¹⁹D. G. Schlom and J. S. Harris, Jr., in *Molecular Beam Epitaxy: Applications to Key Materials*, edited by R. F. C. Farrow (Noyes, Park Ridge, NJ, 1995), pp. 505–622.
- ²⁰C. D. Theis and D. G. Schlom, in *High Temperature Materials Chemistry IX*, edited by K. E. Spear (Electrochemical Society, Pennington, NJ, 1997), Vol. 97-39, pp. 610–616.
- ²¹*Manual for PDA-1024 Detector* (Princeton Instruments, Trenton, NJ, 1997).
- ²²B. J. Gibbons, Ph.D. thesis, The Pennsylvania State University, 1998.
- ²³W. Kern and D. A. Puotinen, *RCA Rev.* **31**, 187 (1970).
- ²⁴P. Lautenschlager, M. Garriga, L. Viña, and M. Cardona, *Phys. Rev. B* **36**, 4821 (1987).
- ²⁵M. Wakagi, B. Hong, H. V. Nguyen, R. W. Collins, W. Drawl, and R. Messier, *J. Vac. Sci. Technol. A* **13**, 1917 (1995).
- ²⁶R. L. Goettler, J.-P. Maria, and D. G. Schlom, in *Epitaxial Oxide Thin Films III*, edited by D. G. Schlom, C. B. Eom, M. E. Hawley, C. M. Foster, and J. S. Speck, *MRS Symposium Proceedings* (Materials Research Society, Pittsburgh, 1997), Vol. 474, pp. 333–338.
- ²⁷R. A. McKee and F. J. Walker, U.S. Patent No. 5,225,031 (6 July 1993).
- ²⁸R. A. McKee and F. J. Walker, U.S. Patent No. 5,482,003 (9 January 1996).
- ²⁹S. W. Chan, *J. Phys. Chem. Solids* **55**, 1137 (1994).
- ³⁰K. Harada, H. Nakanishi, H. Itozaki, and S. Yazu, *Jpn. J. Appl. Phys., Part 1* **30**, 934 (1991).
- ³¹T. Mattheé, J. Wecker, H. Behner, G. Friedl, O. Eibl, and K. Samwer, *Appl. Phys. Lett.* **61**, 1240 (1992).
- ³²H. Behner, J. Wecker, T. Mattheé, and K. Samwer, *Surf. Interface Anal.* **18**, 685 (1992).
- ³³A. Bardal, M. Zwerger, O. Eibl, J. Wecker, and T. Mattheé, *Appl. Phys. Lett.* **61**, 1243 (1992).
- ³⁴A. Bardal, O. Eibl, T. Mattheé, G. Friedl, and J. Wecker, *J. Mater. Res.* **8**, 2112 (1993).
- ³⁵J. Haeni (personal communication).
- ³⁶*Handbook of Chemistry and Physics*, edited by D. R. Lide (Chemical Rubber Corp., Boca Raton, FL, 1993).
- ³⁷Y. Nigara, *Jpn. J. Appl. Phys., Part 1* **7**, 404 (1968).
- ³⁸A. Feldman, X. Ying, and E. N. Farabaugh, *Appl. Opt.* **28**, 5229 (1989).
- ³⁹D. F. Bezuidenhout and R. Pretorius, *Thin Solid Films* **139**, 121 (1986).
- ⁴⁰M. Swarnalatha, A. F. Stewart, A. H. Guenther, and C. K. Carniglia, *Appl. Phys. A: Solids Surf.* **54**, 533 (1992).
- ⁴¹D. Basak and S. K. Sen, *Thin Solid Films* **254**, 181 (1995).
- ⁴²*Powder Diffraction File* (International Center for Diffraction Data, Swarthmore, PA, 1995), JCPDS card No. 43-631.